1.E.4

Nuclear Physics A255 (1975) 221–242; © *North-Holland Publishing Co., Amsterdam*

PRECISION LIFETIME MEASUREMENTS WITH THE COINCIDENT HIGH-VELOCITY DSA METHOD IN INVERSE REACTIONS

J. A. J. HERMANS, G. A. P. ENGELBERTINK, M. A. VAN DRIEL
H. H. EGGENHUISEN and D. BUCURESCU†

Fysisch Laboratorium, Rijksuniversiteit, Utrecht, The Netherlands

Received 30 June 1975

Abstract: Mean lives of low-lying states of ^{18}O, ^{30}Si, ^{33}S and ^{34}S have been measured with the Doppler-shift attenuation method by heavy-ion bombardment of ^{2}H and ^{3}H targets. The γ-ray Doppler patterns are observed with a large Ge(Li) detector at 0° in coincidence with protons around 180°, so that the experiments are performed with high-velocity, mono-energetic and unidirectional beams of nuclei in well-defined excited states. Interpretation of the γ-ray patterns measured with Mg, Al, Cu and Ag as slowing-down material, with accurately known experimental stopping powers yields consistent results with small errors: ^{18}O, τ_m (1.98 MeV) = 2790 ± 110 fs; ^{30}Si, τ_m(2.24) = 351 ± 19 fs and τ_m(3.50) = 89 ± 8 fs; ^{33}S, τ_m(0.84) = 1650 ± 50 fs and τ_m(2.31) = 206 ± 8 fs; ^{34}S, τ_m(2.13) = 470 ± 20 fs and τ_m(3.30) = 196 ± 13 fs. The deduced transition strengths are compared with results from large-scale shell-model calculations.

E NUCLEAR REACTIONS ^{3}H(^{16}O, pγ), E = 20 MeV; ^{3}H(^{28}Si, pγ), E = 33 MeV; ^{2}H(^{32}S, pγ), E = 38 MeV; ^{3}H(^{32}S, pγ), E = 38 MeV; measured γ-ray Doppler patterns. ^{18}O, ^{30}Si, ^{33}S, ^{34}S levels deduced τ_m, transition strengths.

1. Introduction

Several lifetime measurements [1, 2]) in recent years have shown the results obtained with the Doppler-shift attenuation method to be strongly dependent on the slowing-down material. A most illustrative example is the wide range of values from 0.29 to 0.54 ps for the lifetime of ^{22}Ne(3.34 MeV), measured by Broude *et al.* [3]) with 39 different backing materials.

The large systematic deviations observed may probably be attributed to two main causes, both stemming from the low initial recoil velocities ($v \approx 0.01\,c$) generally involved. (i) Lack of information on experimental stopping powers at low velocities often forces previous work to rely on the theoretical stopping cross sections of Lindhard *et al.* [4]), as worked out by Blaugrund [5]). (ii) Due to the short range in the slowing-down material the results are most sensitive to surface effects and local disturbances. Also the uncertain atomic composition and density of some chemical compound targets can be rather troublesome.

† Permanent address: Institute of Atomic Physics, P.O. Box 5206, Bucharest, Rumania.

The higher initial velocities required to overcome these problems may be obtained from inverse reactions in which very light nuclei like ^{1}H, ^{2}H, ^{3}H and ^{4}He are bombarded with heavy ions[6-8]). At high recoil velocities ($v > 0.01\,c$) the stopping power of heavy ions in several materials is accurately known experimentally; the electronic stopping power dominates here the slowing-down process whereas the nuclear stopping power, which is difficult to treat and not well investigated, affects only the last part of the path of the ions.

The high initial velocities also mean that the recoiling nuclei spend little time in the target (with its often uncertain properties) and quickly reach the backing, for which a wide choice of slowing-down materials is available. Furthermore the Doppler effect at 0° is large compared to the 2–3 keV resolution of a Ge(Li) detector. Thus the Doppler pattern, which for a given lifetime reflects the slowing-down process, can be studied in detail.

Detection of the γ-radiation in coincidence with the outgoing particles enables the selection of the excited state of the nuclei. This not only excludes feeding from higher levels, but also greatly reduces background. The coincidence restriction confines the contributing nuclei to a narrow cone of about 1° half-angle. Since the initial velocity spread is small too ($\Delta v/v \approx 0.01$), the recoils approximate a high-velocity, mono-energetic and uni-directional beam of nuclei in a well-defined excited state.

This paper reports on coincident high-velocity DSA line-shape measurements in which ^{2}H and ^{3}H targets are bombarded with several heavy-ion beams from the Utrecht EN tandem accelerator. Preliminary results presented earlier[7,9-11]) are superseded by the present paper.

2. Experimental method

Thin 200 $\mu g/cm^2$ TiD and TiT targets on a 0.3 mm thick backing are bombarded with $^{16}O^{3+}$, $^{28}Si^{5+}$ and $^{32}S^{6+}$ beams. The tritium targets have a (protective) layer of 45 $\mu g/cm^2$ Al or Au. During an experiment the target spot was changed about every two hours to prevent carbon build-up and radiation damage. The carbon build-up would e.g. give rise to particles from ^{12}C(HI, $xn\,yp\,z\alpha$) reactions. So far as their stopping properties are concerned the backing materials Mg, Al and Cu are

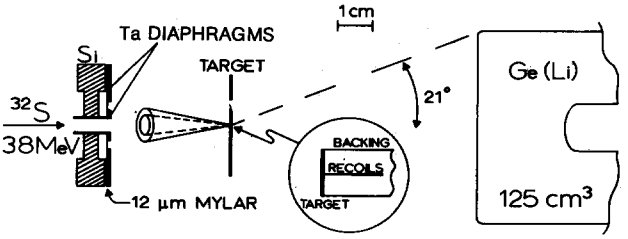

Fig. 1. The experimental set-up. The solid angle of the particle detector amounts to 75 msr. The recoiling nuclei are moving forward within a cone of 0.6° half-angle.

in the approximate ratio of 1 : 2 : 3, with Mg being the softest; Ag resembles Cu in this respect. The bombarding energies used produce nuclei recoiling at an initial velocity of $v/c \approx 0.05$.

The experimental set-up is shown in fig. 1. The γ-ray patterns are observed with a 25% efficient Ge(Li) detector at 0° in coincidence with protons. The latter are detected in an annular Si counter at 180° which is shielded from elastically scattered beam particles by a 12 μm thick mylar foil. These positions are most favourable with respect to the following. At 0° the Doppler pattern is widest and the geometrical smearing, due to the finite solid angle of the detector, is smallest. Although the solid half-angle of the γ-detector amounts to 21°, the variation of the cosine over the solid angle is only 7%. At the position on the axis the solid angle of the Si detector causes the smallest kinematical broadening of the particle spectrum, as illustrated in fig. 2 for the p_1 group in the $^2H(^{32}S, p)^{33}S$ reaction. In the experiments solid angles between 75 and 150 msr were used for the particle detector.

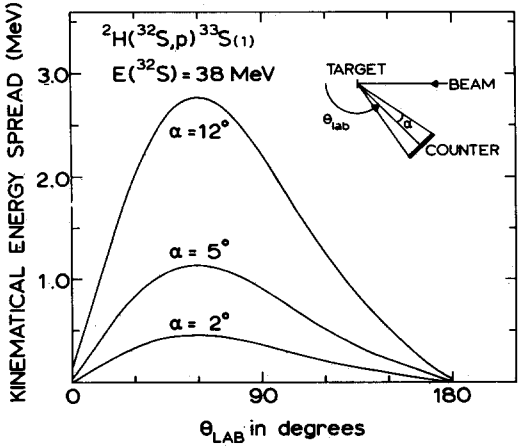

Fig. 2. Kinematical broadening of the p_1 group in the reaction $^2H(^{32}S, p)^{33}S(1)$ at 38 MeV as a function of detector position for three different solid half-angles. The point at $\theta_{lab} = 180°$ on the $\alpha = 12°$ curve represents the experimental situation.

The resolution of the particle spectra is determined by several effects, of which the kinematical energy spread due to the solid angle contributes most. Other contributions stem from detector resolution, target thickness and straggling in the 12 μm mylar foil.

Event-mode recording techniques were used employing a CDC 1700 computer and standard electronics. Windows on energy and time ($\approx$ 5 ns FWHM, see fig. 3) were set to select only those events that correspond to the direct population of the level under study. A typical value for the time it takes to record a spectrum is that of the $^2H(^{32}S, p\gamma)^{33}S$ measurement with the Mg backing, namely about 50 hours at a beam intensity of 250 nA (electrical).

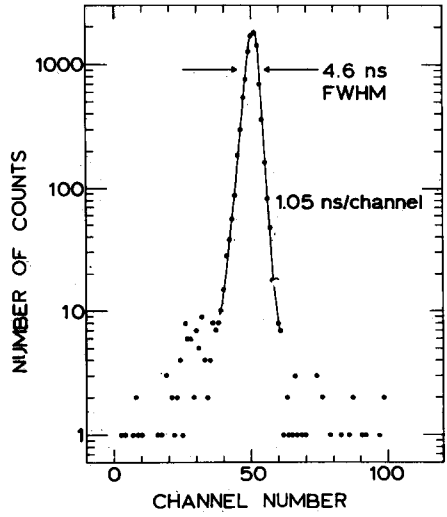

Fig. 3. Time spectrum for the 840 keV $^{33}S(1 \rightarrow 0)$ transition i coincidence with tne p_1 group in the reaction $^{2}H(^{32}S, p\gamma)^{33}S$.

3. Analysis

The energy loss of the recoiling nuclei in the target and backing material was assumed to consist of a nuclear part, $-[dE/d(\rho x)]_n$, which becomes important at low velocities, and an electronic part, $-[dE/d(\rho x)]_e$, dominating the major part of the slowing-down process because of the high initial recoil velocities involved. The total stopping power then is given by

$$-\left[\frac{dE}{d(\rho x)}\right] = -\left[\frac{dE}{d(\rho x)}\right]_n - \left[\frac{dE}{d(\rho x)}\right]_e. \tag{1}$$

The nuclear stopping power, which is not well known experimentally, is parametrized [6]) as $-[dE/d(\rho x)]_n = K_n/(v/v_0)$ where v is the recoil velocity and $v_0 = \frac{1}{137}c$. Values for K_n were obtained by using Bohr's estimate [12]) of the nuclear stopping power at $v = v_0$. The lifetime results were found to be rather insensitive to K_n.

Values for the electronic stopping power were taken from the semi-empirical compilation of Northcliffe and Schilling [13]). Their results were fitted with the analytical functions

$$-\left[\frac{dE}{d(\rho x)}\right]_e = \begin{cases} K_e(v/v_0) - K_3(v/v_0)^3 & \text{for } (v/v_0) \leqq (v/v_0)_g \quad (2a) \\ A + B(v/v_0) - C(v/v_0)^2 - K_n/(v/v_0) & \text{for } (v/v_0)_g < (v/v_0). \quad (2b) \end{cases}$$

The constraint that both $-[dE/d(\rho x)]_e$ and its derivative be continuous at $v/v_0 = (v/v_0)_g$ imposes two relations upon the six parameters. Therefore K_e, K_3, $(v/v_0)_g$

and A are chosen as independent parameters, while B and C are calculated from the relations

$$B = 3K_n/(v/v_0)_g^2 + K_e + K_3(v/v_0)_g^2 - 2A/(v/v_0)_g, \tag{3a}$$

$$C = 2K_n/(v/v_0)_g^3 + 2K_3(v/v_0)_g - A/(v/v_0)_g^2. \tag{3b}$$

In order to reproduce the Northcliffe-Schilling results as well as possible, the electronic stopping power data were fitted only over the velocity range of interest for the present work, i.e. $(v/v_0) < 7.1$. For the ions and slowing-down materials used the parameters of eq. (2) have been collected in table 1. These values reproduce the Northcliffe and Schilling data for $(v/v_0) < 7.1$ with an accuracy of about 1%, as can be seen from the last column of table 1.

The expressions for the total stopping power follow from eq. (1) and (2):

$$-\left[\frac{dE}{d(\rho x)}\right] = \begin{cases} K_n/(v/v_0) + K_e(v/v_0) - K_3(v/v_0)^3 & \text{for } (v/v_0) \leqq (v/v_0)_g \quad (4a) \\ A + B(v/v_0) - C(v/v_0)^2 & \text{for } (v/v_0)_g < (v/v_0). \quad (4b) \end{cases}$$

In order to arrive at eq. (4b) without introducing an unnecessary discontinuity in the total stopping power, the term $-K_n/(v/v_0)$ has been included in eq. (2b) of the parametrization of the electronic stopping power. Since K_n depends on the atomic weight of the recoiling ion the stopping power parameters are slightly different for different isotopes, as can be seen e.g. in table 1 for the energy loss of ^{33}S and ^{34}S. The analytical expressions for the pattern that can be derived from eqs. (4a) and (4b) assuming no change in direction of the recoiling nuclei, have been given explicitly by Warburton *et al.* in eq. (B14) of ref. [14]) and eq. (5) of ref. [6]), respectively.

In the calculation of the theoretical pattern it is assumed that all recoiling nuclei originate from the middle of the thin target. Normalization of the different parts of the pattern upon leaving the target or reaching $(v/v_0)_g$ is accomplished by demanding the number of still excited nuclei to be a continuous function of the recoil velocity.

The following effects are incorporated in the analysis.

(i) *Geometrical smearing.* Because of the finite solid angle of the Ge(Li) detector the γ-radiation is detected between $-21°$ and $+21°$. To account for this geometrical smearing the detection probability has to be considered as a function of the angle between the direction of the γ-ray and the beam direction. This probability was taken proportional to $1 - \exp[-\mu(E)x]$ where x is the path length in the crystal and $\mu(E)$ the absorption coefficient. Due to the solid angle the γ-ray intensity is integrated over energy from $E_\gamma[1 + 0.93\beta(t)]$ to $E_\gamma[1 + \beta(t)]$ with the geometrical smearing function as weight. This yields for $E_\gamma = 1$ MeV and $\beta(0) = 0.05$ an initial integration width of 3.5 keV for the high-energy side of the pattern. So the spatial integration over the solid angle of the Ge(Li) detector corresponds energywise to an integration interval comparable to or smaller than the FWHM of the detector response function. The width of the integration interval shrinks with decreasing $\beta(t)$, resulting in a δ-

TABLE 1

Parameters for the energy loss of ions with $v < 7.1\, v_0$ [a])

Ion	Stopping material	K_n [b]) (keV·cm²/μg)	K_e (keV·cm²/μg)	K_3 (keV·cm²/μg)	$(v/v_0)_g$	A (keV·cm²/μg)	B [c]) (keV·cm²/μg)	C [c]) (keV·cm²/μg)	D^2 [d])
^{18}O	Mg	0.200	2.976	0.065	3.802	5.329	1.153	0.132	1.05
	Al	0.188	2.847	0.066	3.602	4.530	1.230	0.133	1.08
	Ti	0.152	1.897	0.031	4.500	4.311	0.623	0.066	2.65
^{30}Si	Ti	0.427	2.504	−0.027	1.897	−0.983	3.799	0.296	0.76
	Cu	0.391	1.954	−0.039	1.997	−1.242	3.337	0.254	0.69
^{33}S	Mg	0.699	4.329	−0.005	1.796	−0.889	5.951	0.497	1.09
	Al	0.659	4.154	−0.001	1.597	−0.260	5.253	0.422	1.09
	Ti	0.541	2.726	−0.032	1.998	−1.225	4.230	0.314	0.63
	Cu	0.497	2.139	−0.043	1.998	−1.167	3.508	0.244	0.47
	Ag	0.386	1.710	−0.035	1.998	−0.966	2.827	0.199	0.64
^{34}S	Al	0.662	4.155	−0.001	1.597	−0.257	5.251	0.422	1.09
	Ti	0.544	2.726	−0.032	1.998	−1.222	4.229	0.314	0.63
	Cu	0.500	2.139	−0.043	1.998	−1.164	3.507	0.244	0.47

[a]) The parametrization is discussed in the text (see eqs. (4a) and (4b)).

[b]) Bohr's estimate, see text.

[c]) The continuity condition for the stopping power and its derivative at $(v/v_0)_g$ yields two equations for the six parameters. Therefore B and C are calculated from the four other parameters with eqs. (3a) and (3b) in the text.

[d]) $D^2 \equiv 1/(N-4)\sum_i{}^N[\{(\mathrm{d}E/\mathrm{d}(\rho x))_{ei}^{par} - (\mathrm{d}E/\mathrm{d}(\rho x))_i^{NS}\}/0.01(\mathrm{d}E/\mathrm{d}(\rho x))_i^{NS}]^2$ with $N = 25$.

function for the stopped peak. The geometrical smearing function for a 0.84 MeV γ-ray and the present set-up is shown in fig. 4.

From the considerations above also follows that possible angular correlation effects will hardly distort the pattern. For an angular correlation of the form $W(\theta) = 1 + A_2 P_2 (\cos \theta)$ the relative intensity variation over the solid angle of the Ge(Li) detector is given by $[W(0°) - W(21°)]/W(0°) \approx A_2/(5 + 5A_2)$. For $A_2 = 0.3$ this results in an intensity variation of less than 5% over the energy integration interval mentioned above. Its influence would be detectable first at the high-energy end of the pattern for high-energy γ-rays. Formally the angular correlation function $W(\theta)$ can be incorporated in the directional efficiency function of fig. 4. In the present work $W(\theta)$ is taken to be constant over the solid angle of the Ge(Li) detector.

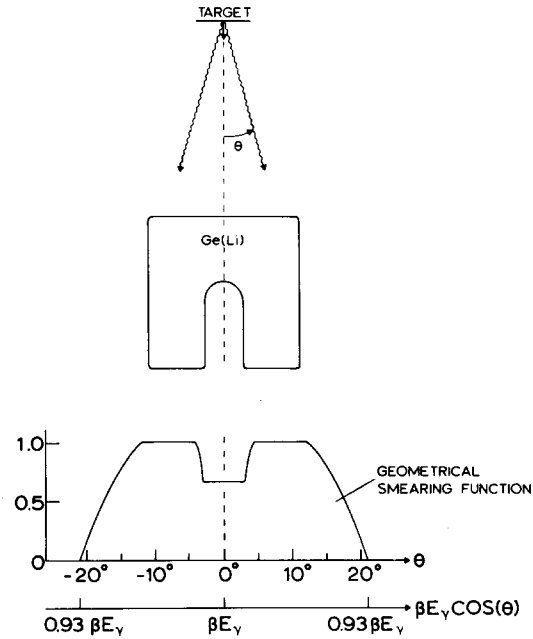

Fig. 4. Geometrical smearing function for the set-up of fig. 1 and a 840 keV γ-ray. The straight arrow on the axis of symmetry indicates the direction of the recoiling nuclei. The solid-angle reduction coefficients $Q^{(1)}$ and $Q^{(2)}$, depend weakly on the γ-ray energy for γ-rays between 0.5 and 2.5 MeV (see table 2).

(ii) *Detector response function.* After applying geometrical smearing the theoretical pattern has to be folded with the intrinsic detector response function. For the description of this function three components were used: a Gaussian, an exponential and a step function. The analytical expressions are given by

$$R(E, E_0) = \begin{cases} H \exp\left[-(E-E_0)^2/2\sigma^2\right] & \text{for } E_0 \leqq E \quad (5a) \\ (H-B) \exp\left[-(E-E_0)^2/2\sigma^2\right] + B & \text{for } E_0 - T \leqq E < E_0 \quad (5b) \\ (H-B) \exp\left[T\{2(E-E_0)+T\}/2\sigma^2\right] + B & \text{for } E < E_0 - T, \quad (5c) \end{cases}$$

where E_0 is the γ-ray energy, H the peak height and B the height of the flat Compton ridge (see fig. 5). Because at energies below E_0 a flat Compton ridge B is added, the normalization factors of the two Gaussians in eqs. (5a) and (5b) have to be slightly different to ensure continuity. At $E = E_0 - T$ there is a smooth transition from a Gaussian to an exponential function to account for a low-energy tail in the response function. The parameters T, σ and B/H were determined from fitting to calibration spectra.

The parametrization given above describes the detector response above the Compton edge. Hence it is only applicable if the Compton edge of the fully shifted part of the pattern is well below the stopped peak, which can be expressed by the condition that $E_\gamma \beta(0) < 511/[2+511/E_\gamma(1+\beta(0))]$ with E_γ the energy of the unshifted γ-ray in keV and $c\beta(0)$ the initial recoil velocity. For the present work this leads to $E_\gamma \lesssim 4.8$ MeV.

(iii) *Higher-order terms in* β. At the velocities involved ($\beta \approx 0.05$) relativistic effects are no longer negligible. The energy of a γ-ray emitted at an angle θ relative to the direction of motion of the nucleus travelling at velocity $v(t) = c\beta(t)$ is given by $E_\gamma(v, \theta)/E_\gamma(v = 0) = \sqrt{1-\beta(t)^2}/[1-\beta(t)\cos\theta]$, which to second order in $\beta(t)$ leads to

$$E_\gamma(v, \theta)/E_\gamma(v = 0) = 1+\beta(t)\cos\theta+\beta^2(t)[\cos^2\theta-\tfrac{1}{2}]. \quad (6)$$

Since for the set-up of fig. 1 $\cos\theta$ is always close to unity (see also sect. 4 eq. (7)) the ratio between second-order and first-order terms is about $\frac{1}{2}\beta$. Thus for the γ-ray pattern an alinearity of less than 2.5% is introduced in the relation between energy (i.e. channel number) and velocity.

(iv) *Lorentz and efficiency corrections.* Due to the motion of the recoiling nuclei the solid angle of the Ge(Li) detector is larger for higher values of β. This Lorentz correction factor of $(1+\beta)/(1-\beta)$ has been combined with an E_γ^{-1} energy dependence for the variation of the detector efficiency over the pattern to give a resulting correction factor of $(1+\beta)$ which the theoretical lineshape has to be multiplied with.

Finally it should be noted that, due to the rapid ($\approx 10^{-16}$ s) filling of electron orbits during the slowing-down process, effects related to hyperfine interactions play no role in this kind of measurements as opposite to e.g. recoil-distance type experiments.

A set of possible γ-ray patterns as a function of the mean life τ_m calculated with the present formalism is shown in fig. 6 for Mg as slowing-down material. The same shapes also apply (in first approximation) to Al and Cu as slowing-down material if the indicated values for τ_m are divided by factors of 2 and 3, respectively.

A lower limit to the lifetimes that can be measured with the present set-up is set by the target thickness. The 0.44 μm thickness of the 200 μg/cm^2 target corresponds for $\beta = 0.05$ to a crossing time of about 29 fs. For a mean life of 20 fs and a uniform cross section throughout the target about half of the excited nuclei will decay in the target with its uncertain slowing-down properties. For $\tau_m = 50$ fs the number of excited nuclei decaying in the backing is about 75%. These considerations

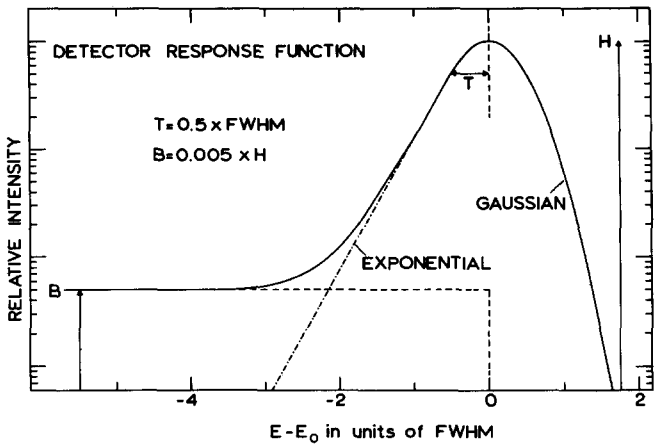

Fig. 5. Detector response function and its components for realistic values of the parameters. Explicit formulas are given in the text (eq. (5)). The parameters T, FWHM and B/H are determined from fitting to calibration spectra.

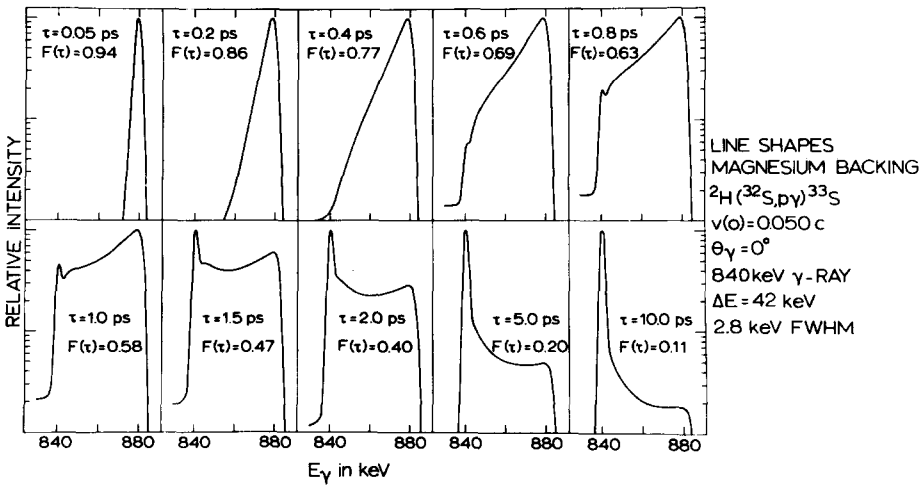

Fig. 6. A set of possible γ-ray patterns with Mg as slowing-down material as a function of the mean life. The same shapes also apply (in first approximation) to Al and Cu as a slowing-down material if the indicated values for τ_m are divided by factors of 2 and 3, respectively.

show that with the targets presently used no reliable results can be obtained for lifetimes shorter than about 40 fs. The shortest mean life reported in the present work is 89 fs.

4. Results

A survey of all results is given in table 3. The theoretical pattern was fitted to the experimental data in a least-squares procedure by varying the mean life τ_m and the

width of the pattern. The width ΔE is given by

$$\Delta E = E_0[Q^{(1)}\beta(0)+\tfrac{1}{2}Q^{(2)}\beta(0)^2], \tag{7}$$

and yields for known γ-ray energy E_0 and solid-angle reduction coefficients $Q^{(1)}$ and $Q^{(2)}$ (see table 2) the initial recoil velocity $c\beta(0)$.

The results for $\beta(0)$ obtained in this way are given in column 4 of table 3. The errors of less than 0.5% are more than five times smaller than the second-order term in eq. (6). A change of x% in $\beta(0)$ brings about a change of at least x% in τ_m. The $\beta(0)$ values

TABLE 2

Solid-angle reduction coefficients[a]) for the set-up of fig. 1

E_γ (MeV)	$Q^{(1)}$	$Q^{(2)}$
0.5	0.9826	0.9317
1.0	0.9831	0.9335
1.5	0.9833	0.9343
2.0	0.9834	0.9347
2.5	0.9835	0.9350

[a]) The solid-angle reduction coefficients, $Q^{(1)}$ and $Q^{(2)}$, are obtained by averaging $\cos\theta$ and $2(\cos^2\theta-\frac{1}{2})$, respectively, over the solid angle of the Ge(Li) detector with the geometrical smearing function as weight.

are furthermore in good agreement with those calculated from the kinematics under the assumption of a uniform cross section over the stated † target thickness.

The results for τ_m given in column 12 will be discussed separately in the following sections.

The attenuation factor $F(\tau_m)$, defined as the normalized centroid of the pattern, is given by

$$F(\tau_m) = \int v \frac{dN(v)}{dv}\,dv \Big/ v(0)\int \frac{dN(v)}{dv}\,dv,$$

with $dN(v)/dv$ the number of nuclei deexciting at recoil velocity v. The quite different values of $F(\tau_m)$ obtained for the same τ_m with different slowing-down materials, reflect the large variations observed in the γ-ray patterns. The attenuation factors for the data points and the calculated shape are listed in columns 6 and 7 of table 3, respectively. Their mutual agreement is good, as expected already from the χ^2 values for the fit in column 8.

The error ΔF in $F(\tau_m)$ is compounded from the uncertainties in (i) the centroid of

† Nukem, Hanau, W. Germany.

TABLE 3

Summary of coincident high-velocity DSA results

Nucleus (E_x in MeV)	Reaction and bombarding energy	E_γ (keV)	$\beta(0)$ (%)	Slowing down material	$F(\tau_m)_{exp}$ (%)	$F(\tau_m)_{fit}$ (%)	χ^2	τ_m (fs)	Statistical error (fs)	Adopted error[a] (fs)	Adopted result[b] (fs)
^{18}O(1.98)	^{3}H(^{16}O, pγ)^{18}O 20 MeV	1982.0	4.88±0.02	Mg	30.8±0.4	30.6	1.1	2821	59	153	2790±110
			4.72±0.02	Al	22.2±0.5	21.5	1.2	2763	77	158	
^{30}Si(2.24)	^{3}H(^{28}Si, pγ)^{30}Si 33 MeV	2235.4	4.79±0.02	Cu	54.0±0.6	54.3	1.5	351	8	19	351± 19
^{30}Si(3.50)	^{3}H(^{28}Si, pγ)^{30}Si 33 MeV	1262.7	4.76±0.02	Cu	82.1±1.2	84.5	1.2	89	7	8	89± 8
^{33}S(0.84)	^{2}H(^{32}S, pγ)^{33}S 38 MeV	840.4	5.05±0.02	Mg	42.7±0.5	42.5	1.1	1659	35	90	1650± 50
			5.04±0.02	Al	32.7±0.4	32.8	1.0	1646	31	88	
			4.95±0.02	Cu	19.3±0.3	19.5	1.5	1596	32	86	
			4.95±0.02	Ag	19.3±0.3	19.6	2.0	1705	35	92	
^{33}S(2.31)	^{2}H(^{32}S, pγ)^{33}S 38 MeV	1471.7	5.01±0.02	Al	80.0±0.9	80.6	1.6	198	11	15	206± 8
			4.91±0.02	Cu	68.2±0.9	68.7	0.9	201	8	13	
			4.91±0.02	Ag	67.6±1.0	67.3	1.1	221	10	15	
^{34}S(2.13)	^{3}H(^{32}S, pγ)^{34}S 38 MeV	2127.3	4.72±0.02	Al	64.3±1.3	65.1	1.1	450	25	34	470± 20
			4.88±0.02	Cu	46.1±0.8	46.2	1.0	490	15	29	
^{34}S(3.30)	^{3}H(^{32}S, pγ)^{34}S 38 MeV	1176.1	4.70±0.02	Al	78.8±1.5	79.3	1.0	201	18	21	196± 13
			4.86±0.02	Cu	65.4±1.5	67.6	1.1	193	13	16	

[a]) Quadratic addition of statistical error and 5% stopping power error.
[b]) See text.

the pattern, (ii) the position of E_0 and (iii) the value of $\beta(0)$. For all measurements the largest contribution stems from (i). So the error ΔF is mainly determined by the total area of the pattern. It leads to the statistical error $(\Delta\tau_m)_{stat}$ in the mean life τ_m via

$$(\Delta\tau_m)_{stat}/\tau_m = \Delta F/F(1-F). \tag{8}$$

A small error in $F(\tau_m)$ is therefore a prerequisite for an accurate lifetime measurement. For a given mean life and area the smallest $(\Delta\tau_m)_{stat}$ is obtained with that slowing-down material which will give $F(\tau_m) = 0.5$. The errors $(\Delta\tau_m)_{stat}$ are listed in column 10 of table 3.

The background underneath the pattern is in general negligible for the present clean coincidence experiments as will be discussed in the following sections with specific results.

A more fundamental source of error stems from the imperfect knowledge of the $-dE/d(\rho x)$ and for the present high-velocity measurements more specifically of the electronic stopping power. A change of $x\%$ in the electronic stopping power data used will induce a $x\%$ change of opposite sign in τ_m.

On the basis of recent measurements [15]) of stopping powers for ^{4}He, ^{16}O and ^{35}Cl ions at 1–3 MeV per nucleon and investigations [16]) of the effective charge concept we have adopted an error of 5% in the phenomenological stopping power results of Northcliffe and Schilling [13]). Also the good internal consistency in the present work for $\tau_m[^{33}S(1)]$ results obtained with the slowing-down materials Mg, Al, Cu and Ag shows that the *relative* stopping powers of ref. [13]) are correct to about $(3\pm2)\%$. Information about the *absolute* magnitude of the stopping power should be obtained from a comparison of the present results with those from non-DSA techniques (see subsect. 5.1).

The influence of the nuclear stopping power is small and obviously affects the longer mean lives more than the shorter ones. A (reasonable) change of 20% in the value of K_n has a less than 2% effect on the reported mean lives. This shows that for the present purpose the simple first-order description of the nuclear stopping power is quite adequate.

Quadratic addition of the statistical error $(\Delta\tau_m)_{stat}$ and a stopping power error of $0.05\,\tau_m$ gives the adopted error of column 11 in table 3. The adopted result in column 12 is the weighted mean of the τ_m values measured with the different slowing-down materials with the values of column 11 as weights. The internal error belonging to these weights, which in all cases is larger than the corresponding external error, has been adopted as the final error listed in column 12. This implies that the error in the adopted result is taken inversely proportional to the square root of the number of slowing-down materials used. The results will now be looked into in some more detail.

4.1. THE REACTION $^{3}H(^{16}O, p\gamma)^{18}O$

A 200 $\mu g/cm^2$ TiT target was bombarded with a 20 MeV $^{16}O^{3+}$ beam. The reaction has a rather low Q-value of 3.71 MeV.

As a relatively long lifetime [17]) of a few ps is involved only the soft backing materials Mg and Al were used to slow down the ^{18}O ions. The pattern of the 1982 keV transition from the first excited state to the ground state recorded with the Mg backing is shown in fig. 7. The background of 2.6 counts per channel, which is visible to the

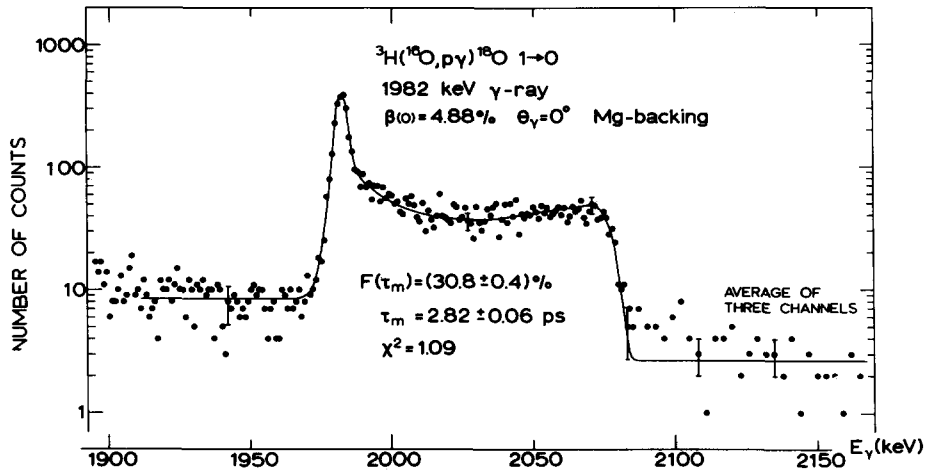

Fig. 7. Doppler γ-ray pattern of the $^{18}O(1 \rightarrow 0)$ transition measured with a Mg backing. The solid line represents the least-squares fit to the data, calculated with the stopping powers given by Northcliffe and Schilling [13]), see text. The background of 2.6 counts per channel, which is visible to the right of the pattern, is assumed to be constant. To the left of the stopped peak the accumulated (flat) Compton contributions from all γ-rays in the pattern raise the level above the background.

right of the pattern, is assumed to be constant. To the left of the stopped peak the figure shows the background plus the accumulated (flat) Compton contributions (see eq. (5)) from all γ-rays in the pattern. The total net area amounts to 6300 counts. The solid line represents the least-squares fit to the data. It should be noted that the error in τ_m given in the figure is statistical only. Because Al is not as soft a material as Mg a greater part of the total area will be contained in the stopped peak, which is reflected in a smaller $F(\tau_m)$ value (see table 3).

The values for τ_m obtained with the Mg and Al backings are in excellent mutual agreement and lead to a mean life of 2790 ± 110 fs for the 1.98 MeV level.

4.2. THE REACTION $^{3}H(^{28}Si, p\gamma)^{30}Si$

The particle spectrum of this inverse (t, p) reaction, with $Q = 10.60$ MeV, is shown in fig. 8. The number of investigated transitions is limited by unresolved proton groups corresponding to excited states with overlapping γ-ray patterns.

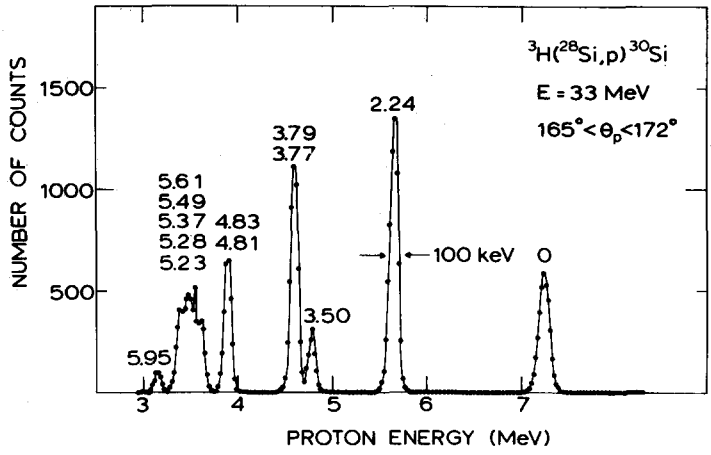

Fig. 8. Particle spectrum of the $^3H(^{28}Si, p)^{30}Si$ reaction. Because of the high Q-value of 10.60 MeV the protons at backward angles have energies up to 7 MeV. The resolution is mainly determined by the solid angle.

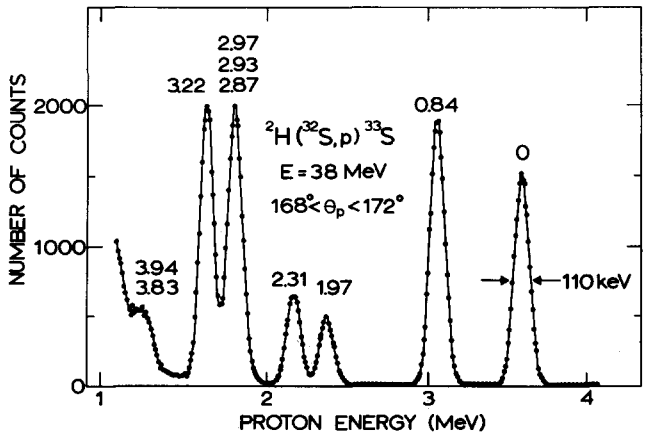

Fig. 9. Proton spectrum produced in the $^2H(^{32}S, p)^{33}S$ reaction. The resolution is mainly determined by the solid angle.

Because of the relatively short lifetimes involved a Cu backing was used in this experiment. From the transition to the ground state a value of 351 ± 19 fs was extracted for the mean life of the first excited state at 2.24 MeV. The $F(\tau_m)$ of $(54.0 \pm 0.6)\%$ approximates the optimum value of 50% (see eq. (8)). The transition from the second to the first excited state has $F(\tau_m) = (82.1 \pm 1.2)\%$, resulting in a value of 89 ± 8 fs for the mean life of the 3.50 MeV level. The shape of these patterns can be estimated from fig. 6.

4.3. THE REACTION $^{2}H(^{32}S, p\gamma)^{33}S$

Doppler γ-ray patterns are determined both by the lifetime of the level involved and by the slowing-down process. An important test on the reliability of the stopping power used therefore is to repeat the measurement with different backing materials. This was done with the $^{2}H(^{32}S, p\gamma)^{33}S$ reaction ($Q = 6.42$ MeV) at a bombarding energy of 38 MeV, the particle spectrum of which is shown in fig. 9.

Four different backing materials were used: Mg, Al, Cu and Ag. For three of these

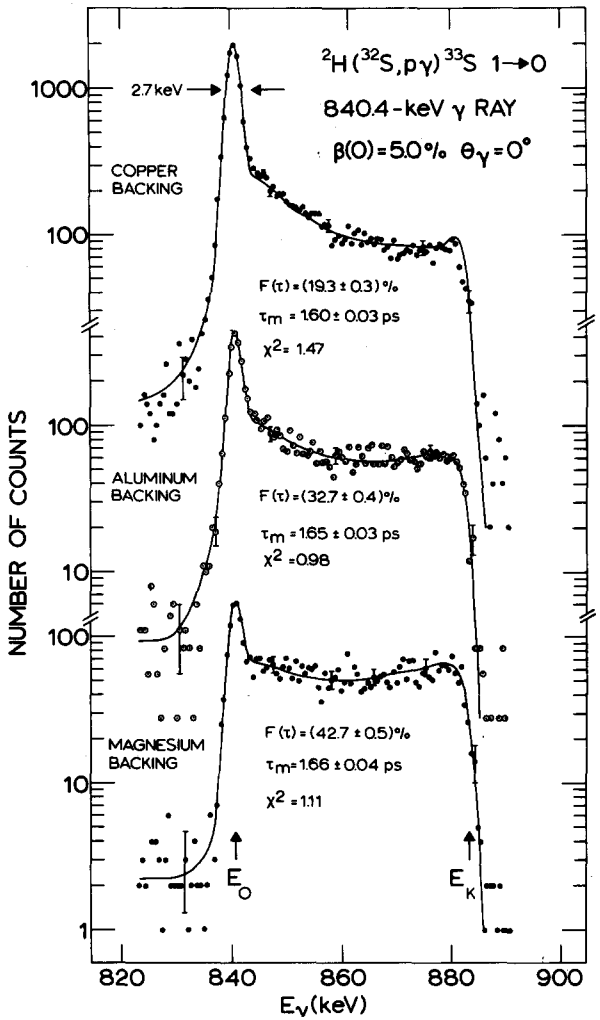

Fig. 10. Doppler γ-ray patterns for $^{33}S(1 \rightarrow 0)$ in slowing-down materials of Mg, Al and Cu; E_0 and E_k denote the positions of stopped and fully shifted peak, respectively. The contribution from randoms and background, less than 0.5 counts per channel, is neglected. The errors given for τ_m are statistical only.

the pattern of the 840 keV transition from the first excited state to the ground state is shown in fig. 10. The net areas amount to 4800, 7000 and 18600 counts for Mg, Al and Cu, respectively. The pattern from the Ag backing, which is not shown here, contains 9000 counts. The errors for τ_m given in the figure are statistical only; E_0 and E_k denote the positions of the stopped and fully shifted peak, respectively. The width of the pattern is about 42 keV, many times the detector resolution of 2.7 keV FWHM. Background and randoms amount to only 0.5 counts per channel.

In spite of the quite different slowing-down processes, reflected in the different $F(\tau_m)$ values, the τ_m results, with a statistical accuracy of about 2%, show good consistency (see table 3). Increasing the nuclear stopping power by 20% did not decrease the result from the Cu backing more than 1.6%. The average value adopted for the mean life of the 0.84 MeV level is 1650 ± 50 fs.

The transition from the third to the first excited state was used to determine the mean life of the 2.31 MeV level. The consistent results obtained with Al, Cu and Ag backings lead to a final value of 206 ± 8 fs.

4.4. THE REACTION $^3H(^{32}S, p\gamma)^{34}S$

This reaction ($Q = 11.58$ MeV) was carried out at a bombarding energy of 38 MeV. The resulting proton spectrum is shown in fig. 11.

As the lifetimes of interest were relatively short, Cu and Al were chosen as slowing-down material. The γ-ray patterns for the transition from the first excited state to the ground state have net areas of 2000 and 1750 counts, respectively. Thev are shown

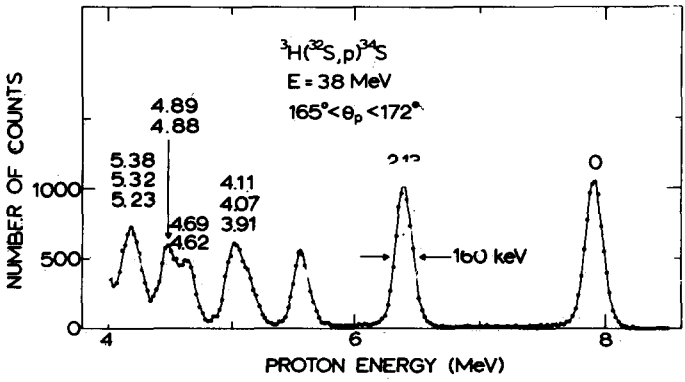

Fig. 11. Particle spectrum of the $^3H(^{32}S, p)^{34}S$ reaction. The resolution is mainly determined by the solid angle.

in fig. 12. A 1.0 count per channel contribution from randoms and background has been subtracted. The result obtained with the Cu backing showed a variation of

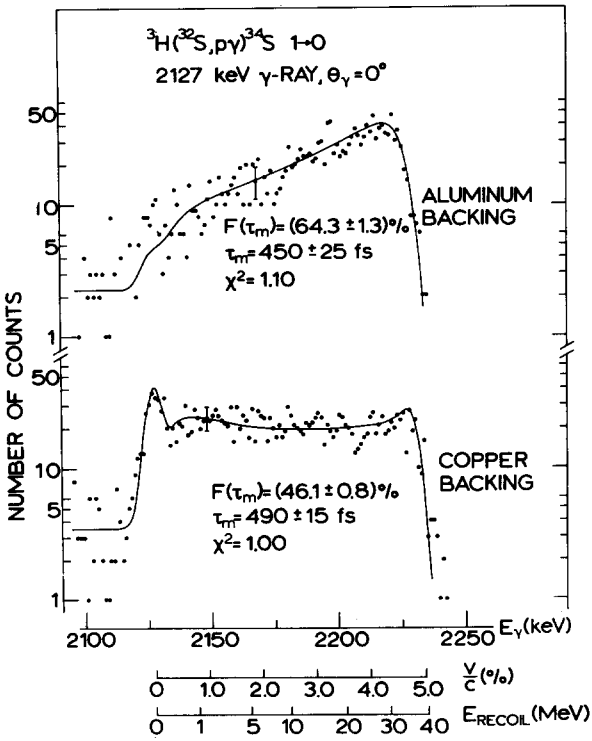

Fig. 12. Doppler γ-ray patterns for the $^{84}S(1 \rightarrow 0)$ transition measured with Al and Cu as backing material. A 1.0 count per channel contribution from randoms and background has been subtracted in each case. The errors given for τ_m are statistical only.

1.0% for 20% change in K_n. The value adopted for the mean life of the 2.13 MeV level is 470 ± 20 fs.

From the patterns of the transition from the third to the first excited state a value of 196 ± 13 fs was extracted for the mean life of the 3.30 MeV level.

5. Discussion

The values from the present work are compared with previous measurements in table 4. Asterisks denote the results from previous experiments employing heavy-ion beams. These are most suitable for comparison, though none but one [22]) comes from a coincident measurement. The values from ref. [23]) are averages of independently obtained results which in general show considerable spread.

The agreement of the Coulomb excitation results of Schwalm *et al.* [16]) is excellent for $^{33}S(1)$ and $^{34}S(1)$ but poor for $^{30}Si(1)$. The result of 370 ± 60 fs from the work of Olin *et al.* [24]) for the mean life of $^{34}S(1)$ differs 1.5 standard deviation from the present value of 470 ± 20 fs.

TABLE 4

Comparison of present mean lives with previous results

Nucleus	E_x (MeV)	τ_m (ps) present	τ_m (ps) previous	Method[a]	Ref.
^{18}O	1.98	2.79 ±0.11	3.40 ±0.34	CE	[18]
			2.73 ±0.05*	CE	[19]
			$2.9^{+0.9}_{-0.6}$	DSA	[20]
			3.58 ±0.18*	RD	[17]
			3.35 ±0.20*	RD	[21]
			2.90 ±0.12*	RD	[22]
^{30}Si	2.24	0.351±0.019	0.34 ±0.03	DSA	[1]
			0.34 ±0.04	DSA	[23]
			0.26 ±0.06*	CE	[16]
	3.50	0.089±0.008	0.100±0.020	DSA	[23]
^{33}S	0.84	1.65 ±0.05	1.70 ±0.15	DSA	[23]
			2.0 ±0.3*	DSA	[6]
			1.69 ±0.18*	CE	[16]
	2.31	0.206±0.008	0.160±0.020	DSA	[23]
^{34}S	2.13	0.470±0.020	0.41 ±0.04	DSA	[23]
			0.37 ±0.06*	CE	[24]
			0.47 ±0.03*	CE	[16]
	3.30	0.196±0.013	0.165±0.020	DSA	[23]

Asterisks denote previous results obtained with heavy-ion beams.

[a]) CE = Coulomb excitation, DSA = Doppler shift attenuation and RD = recoil distance.

The Coulomb excitation result for $^{18}O(1)$ of $B(E2, 0^+ \rightarrow 2^+) = (488 \pm 8) \times 10^{-5} e^2 \cdot b^2$ (corresponding to $\tau_m = 2.73 \pm 0.05$ ps) obtained by Kleinfeld *et al.* [19]) by scattering of ^{18}O projectiles from a thin ^{209}Bi target, agrees perfectly with the present value of 2.79 ± 0.11 ps. The recoil-distance results for this level are discussed in the next section.

5.1. DSAM VERSUS RDM

The use of high recoil velocities in DSA as well as in recoil-distance (RD) measurements has extended the range of both essentially different techniques, so that at present they overlap for the 1–10 ps region. Hence the lifetime of the first excited state in ^{18}O is suitable for a comparison of the two techniques, a detailed discussion of which is given below.

Berant *et al.* [17]) obtained a value of 3.58 ± 0.18 ps in a plunger measurement using the $^{18}O(\alpha, \alpha')^{18}O(1)$ reaction. From their experimental details it is not clear, however, whether the α-particle bombarding energy used was low enough to avoid excitation of the 3.55 MeV, $J^\pi = 4^+$ level, which has a mean life of 25 ps and decays 100% to the first excited state. Even a small amount of feeding from this long-lived level would

result in an increased apparent lifetime of the first excited state.

Another RD measurement by McDonald *et al.*[21]), employing the inverse (t, p) reaction as in the present work, resulted in a value of 3.35 ± 0.20 ps. Feeding from the second excited state was accounted for in this singles measurement, but of the 21 plunger distances used only four are determinative for the lifetime of the first excited state.

A third RD measurement has been performed recently by Asher *et al.*[22]) with the $^{1}H(^{18}O, p)^{18}O(1)$ reaction at a bombarding energy of 47.3 MeV. Population of higher-lying ^{18}O levels is excluded at this energy, equivalent to 2.63 MeV for the normal (p, p′) reaction. The result of 2.90 ± 0.12 ps from several runs at many target-stopper distances has to be compared with 2.79 ± 0.11 ps from the present work. For these two results the ratio τ_m^{RD}/τ_m^{DSA} would amount to 1.04 ± 0.06.

A similar comparison can be made for the mean life of $^{24}Mg(1)$. The weighted average of two accurate, recent DSA measurements, 1.82 ± 0.14 ps [ref. [8])] and 1.92 ± 0.10 ps [ref. [16])], is 1.89 ± 0.08 ps while the weighted average of two accurate RD measurements, 2.11 ± 0.16 ps [ref. [25])] and 2.09 ± 0.13 ps [ref. [26])], is 2.10 ± 0.10 ps. So the ratio τ_m^{RD}/τ_m^{DSA} for $^{24}Mg(1)$ would be 1.11 ± 0.07.

These results do not exclude the possibility that τ_m^{RD} is slightly larger than τ_m^{DSA}, a suggestion worthwhile to be checked with improved experimental accuracy and for more cases because of its implications.

Another (less accurate) comparison[27]) between RDM and DSAM for ^{49}V ions slowing down in Ti, yielded the conclusion $\tau_m^{RD}/\tau_m^{DSA} = 1.0 \pm 0.3$.

5.2. COMPARISON WITH MODEL CALCULATIONS

The results from the present work have been used for comparing experimental transition strengths with theoretical calculations in table 5. Where necessary, branchings and mixing ratios have been taken from ref. [23]).

Five out of the 15 transition strengths listed are pure ($2^+ \rightarrow 0^+$) E2 transitions, so that experimentally the strength is solely determined by the mean life and the branching ratio. For the four mixed M1/E2 transitions the absolute value of the mixing ratio is less than 0.2, so that the E2 admixture of less than 4% hardly affects the M1 strength. The appreciable errors in the mixing ratios, however, result in large errors for the admixed E2 strengths. Therefore table 5 contains only nine transitions with an experimental error smaller than 10% in the strength.

For ^{18}O the best agreement with experiment is obtained by McGrory[30]) with an excited-core calculation. All other calculations yield too low a strength.

For the three (s, d) shell nuclei two sets of shell-model calculations are available. One[31]) uses a *modified* surface delta interaction in a model space taking into account all $2s_{\frac{1}{2}}$ and $1d_{\frac{3}{2}}$ states and up to two holes in the $1d_{\frac{5}{2}}$ shell, and the other[32]) uses a *free-parameter* surface delta interaction in the same model space. In general the two calculations give very similar results.

TABLE 5

Comparison of transition strengths with theoretical calculations

Nucleus	$E_i \to E_f$ (MeV)	$J_i^\pi \to J_f^\pi$	τ_m (ps)	Branching (%)	$\lvert\delta\rvert$	Multi-polarity	Strength (W.u.) exp	Strength (W.u.) theory	ref.
^{18}O	$1.98 \to 0$	$2_1^+ \to 0_1^+$	2.79 ± 0.11	100	0	E2	3.34 ± 0.13	1.1	[28]
								1.8	[29]
								4.3	[30]
^{30}Si	$2.24 \to 0$	$2_1^+ \to 0_1^+$	0.351 ± 0.019	100	0	E2	7.4 ± 0.4	4.5	[31]
								3.1	[32]
	$3.50 \to 0$	$2_2^+ \to 0_1^+$	0.089 ± 0.008	47 ± 2	0	E2	1.45 ± 0.14	1.8	[31]
								2.5	[32]
	$3.50 \to 2.24$	$2_2^+ \to 2_1^+$	0.089 ± 0.008	53 ± 2	0.18 ± 0.04	M1	$(0.50 \pm 0.05) \times 10^{-2}$	16×10^{-2}	[31]
						E2	3.2 ± 1.8	5.4	[31]
								5.0	[32]
^{33}S	$0.84 \to 0$	$(\frac{1}{2})_1^+ \to (\frac{3}{2})_1^+$	1.65 ± 0.05	100		M1	$(3.14 \pm 0.10) \times 10^{-2}$ [a]	3.1×10^{-2}	[31]
								6.7×10^{-2}	[32]
						E2	4.5 ± 0.9 [a]	5.0	[31]
								3.7	[32]
	$2.31 \to 0$	$(\frac{3}{2})_2^+ \to (\frac{3}{2})_1^+$	0.206 ± 0.008	32 ± 2		M1	$< 0.44 \times 10^{-2}$	0.2×10^{-2}	[31]
								0.95×10^{-2}	[32]
						E2	< 3.3	2.6	[31]
								2.5	[32]
	$2.31 \to 0.84$	$(\frac{3}{2})_2^+ \to (\frac{1}{2})_1^+$	0.206 ± 0.008	68 ± 2	0.11 ± 0.08	M1	$(3.21 \pm 0.17) \times 10^{-2}$	4.3×10^{-2}	[31]
								2.4×10^{-2}	[32]
						E2	$0.7^{+1.4}_{-0.7}$	6.5	[31]
								6.0	[32]
^{34}S	$2.13 \to 0$	$2_1^+ \to 0_1^+$	0.470 ± 0.020	100	0	E2	6.0 ± 0.3	8.4	[31]
								5.3	[32]
	$3.30 \to 0$	$2_2^+ \to 0_1^+$	0.196 ± 0.013	47 ± 2	0	E2	0.74 ± 0.06	0.1	[31]
								0.85	[32]
	$3.30 \to 2.13$	$2_2^+ \to 2_1^+$	0.196 ± 0.013	53 ± 2	0.13 ± 0.04	M1	$(5.1 \pm 0.4) \times 10^{-2}$	1.7×10^{-2}	[31]
								1.8×10^{-2}	[32]
						E2	2.5 ± 1.5	11	[31]
								5.3	[32]

Where necessary, branchings and mixing ratios have been taken from ref. [23]).

[a]) The E2 strength has been deduced from the $B(E2)\uparrow$ value of $(19 \pm 4) \times 10^{-4} e^2 \cdot b^2$ given in ref. [33]). It corresponds to a mixing ratio of $|\delta| = 0.158 \pm 0.017$.

For two of the nine well-determined transition strengths mentioned above the calculated strengths deviate considerably. In ^{30}Si the $2_2^+ \rightarrow 2_1^+$ M1 transition is calculated too strong by a factor of 30 while in ^{34}S the similar $2_2^+ \rightarrow 2_1^+$ M1 transition is calculated too weak by a factor of 3. Considering only the best theoretical result for each of the seven remaining transitions (five of E2 and two of M1 character) one observes that although the calculated strength is within 40% of the experimental value, the average disagreement with experiment in units of standard deviation still amounts to 3.8 (if the calculated results are assumed to have no errors).

These considerations show that model calculations still leave something to be desired.

6. Conclusions

The present work gives seven accurate mean lives with final errors between 3% and 9% for low-lying levels (four first-excited states) in ^{18}O, ^{30}Si, ^{33}S and ^{34}S. They result from analysis of Doppler γ-ray patterns measured with the coincident high-velocity DSA method in inverse reactions.

The coincidence condition avoids delayed feeding and removes troublesome background. The high initial velocity not only allows for existing accurate experimental stopping powers to be used in the interpretation of the data but also results experimentally in a detailed Doppler pattern, which provides a check on the description of the slowing-down process.

The method is applicable for 0.04–10 ps and has for $\tau_m \gtrsim 1$ ps a useful overlap with the recoil-distance method.

For ^{33}S(1) recoils slowed down in Mg, Al, Cu and Ag, mean lives mutually consistent to within (3 ± 2)% are obtained, which implies that the *relative* stopping powers used are correct to that order.

The γ-ray patterns contain, for unknown mean life, no information about the *absolute* value of the stopping powers. A comparison between accurate DSA and RD measurements for ^{18}O(1) and ^{24}Mg(1) leads for the time being to the conclusion that the two methods are consistent to within 10%.

The accurate mean lives now available are a challenge to the large scale shell-model calculations presently being performed [34]).

This work was carried out as a part of the research program of the "Stichting voor Fundamenteel Onderzoek der Materie" (FOM) with financial support from the "Nederlandse Organisatie voor Zuiver Wetenschappelijk Onderzoek" (ZWO).

References

1) W. M. Currie, L. G. Earwaker and J. Martin, Nucl. Phys. **A135** (1969) 325
2) M. Bister, A. Anttila, M. Piiparinen and M. Viitasalo, Phys. Rev. **C3** (1971) 1972
3) C. Broude, F. A. Beck and P. Engelstein, Nucl. Phys. **A216** (1973) 603

4) J. Lindhard, M. Scharff and K. E. Schiøtt, Mat. Fys. Medd. Dan. Vid. Selsk. **33** (1963) no. 14
5) A. E. Blaugrund, Nucl. Phys. **88** (1966) 501
6) E. K. Warburton, J. W. Olness, G. A. P. Engelbertink and T. K. Alexander, Phys. Rev. **C7** (1973) 1120
7) J. A. J. Hermans, G. A. P. Engelbertink, D. Bucurescu, M. A. van Driel and H. H. Eggenhuisen, Phys. Lett. **50B** (1974) 337
8) J. S. Forster, D. Ward, G. J. Costa, G. C. Ball, W. G. Davies and I. V. Mitchell, Phys. Lett. **51B** (1974) 133
9) J. A. J. Hermans, G. A. P. Engelbertink and M. A. van Driel, Proc. Int. Conf. on nuclear structure and spectroscopy, Amsterdam 1974, vol. 1, p. 126
10) J. A. J. Hermans, G. A. P. Engelbertink, M. A. van Driel and H. H. Eggenhuisen, Proc. Int. Conf. on nuclear structure and spectroscopy, Amsterdam 1974, vol. 2, p. 532
11) J. A. J. Hermans and G. A. P. Engelbertink, Verhandlungen der Deutschen Physikalischen Gesellschaft, Den Haag 1975, p. 846
12) N. Bohr, Mat. Fys. Medd. Dan. Vid. Selsk. **18** (1948) no. 8
13) L. C. Northcliffe and R. F. Schilling, Nucl. Data Tables **7** (1970) 233
14) E. K. Warburton, J. W. Olness and A. R. Poletti, Phys. Rev. **160** (1967) 938
15) D. Ward, R. L. Graham and J. S. Geiger, Can. J. Phys. **50** (1972) 2302
16) D. Schwalm, Habilitationsschrift 1973, Heidelberg; and to be published
17) Z. Berant, C. Broude, G. Engler and D. F. H. Start, Nucl. Phys. **A225** (1974) 55
18) D. L. Disdier, O. Häusser, A. J. Ferguson and T. K. Alexander (1972), quoted by A. Christy and O. Häusser, Nucl. Data Tables **11** (1972) 281
19) A. M. Kleinfeld, K. P. Lieb, D. Werdecker, and U. Smilansky, Proc. Int. Conf. on reactions between complex nuclei, Nashville 1974, vol. 1, p. 27
20) J. W. Olness, E. K. Warburton and J. A. Becker, Phys. Rev. **C7** (1973) 2239
21) A. B. Mc.Donald, T. K. Alexander, O. Häusser,G. J. Costa, J. S. Forster and A. Olin, Can. J. Phys. **52** (1974) 1381
22) J. Asher, Oxford University, private communication
23) P. M. Endt and C. van der Leun, Nucl. Phys. **A214** (1973) 1
24) A. Olin, O. Häusser, T. K. Alexander, A. J. Ferguson and W. Witthuhn, Nucl. Phys. **A221** (1974) 555
25) T. K. Alexander and A. Bell, Nucl. Instr. **81** (1970) 22
26) R. E. Horstman *et al.*, Nucl. Phys. **A248** (1975) 291
27) B. Haas, J. Chevallier, N. Schulz, J. Styczen and M. Toulemonde, Phys. Rev. **C11** (1975) 280
28) E. C. Halbert, J. B. McGrory, B. H. Wildenthal and S. P. Pandya, Advances in nucl. phys.vol. 4, ed. M. Baranger and E. Vogt (Plenum Press, New York, 1971)
29) T. Engeland and P. J. Ellis, Nucl. Phys. **A181** (1972) 368
30) J. B. McGrory, Proc. Int. Conf. on nuclear structure and spectroscopy, Amsterdam 1974, vol. 2, p. 73
31) P. W. M. Glaudemans, P. M. Endt and A. E. L. Dieperink, Ann. of Phys. **63** (1971) 134
32) B. H. Wildenthal, J. B. McGrory, E. C. Halbert and H. D. Graber, Phys. Rev. **C4** (1971) 1708
33) D. S. Andreev, A. P. Grinberg, K. I. Erokhina and I. Kh. Lemberg, Izv. Akad. Nauk USSR (ser. fiz.) **25** (1961) 70
34) F. Meurders *et al.*, Utrecht University, to be published;
G. A. Timmer *et al.*, Utrecht University, to be published